

## 出國報告（出國類別：參加國際研討會）

# 2015 The Fourth International Conference on Innovation, Communication and Engineering

服務機關：國立虎尾科技大學光電工程系

姓名職稱：劉代山 教授

派赴國家：中國

出國期間：2015年10月22日至10月29日

報告日期：2016年01月14日

## 摘要

本人此次參與福州大學以及台灣知識創新學會於中國長沙所舉辦 2015 International Conference on Innovation, Communication and Engineering 國際研討會，擔任大會 Program Committee 議程委員，並擔任 Session B2 主持人，期間亦發表一篇文章著作，本次會議將各領域(包含 advanced material science and engineering, information technology, innovation design, communication science and engineering, industrial design, creative design, applied mathematics, computer science, design theory, management science, cultural and creative research, electrical and electronic engineering, mechanical and automation engineering, green technology and architecture engineering 等)，劃分為 21 各 sessions，邀請各界優秀的學者與產官先進參與本次大會，此外，大會更安排兩場邀請演講，更提供本人與相關領域傑出學者及專家學習的機會，並藉由隊會安排的討論時間與語彙學者專家溝通交流，大幅提升本人的學術研究能量與跨領域視野。



## 目的

2015 International Conference on Innovation, Communication and Engineering 國際研討會舉辦地點在中國湖南省湘潭市，本次參加學者專家除了有台灣知名教授外，另有來自美國、英國、日本、韓國、葡萄牙、巴林以及澳洲等國家的學者一同參與本研討會。大會並特別邀請由 James P. Barufaldi 以及王駿發教授分別進行主題演講。各位報告者皆簡報目前的研究內容成果，內容豐富充實，本人亦有發表一篇文章。藉由此次會議不僅有助於提升本實驗室的在研發能量上能見度，藉由與與會專家學者的學術交流，更可以開拓本人的視野並開啟與先進團隊合作研究的契機。

## 過程

本人於10月22日由台灣桃園國際機場搭乘華航(AE977)班機，於湖南當地時間上午11點50分抵達長沙市黃花國際機場，旋即與與會的專家學者搭乘巴士前往此次下榻的飯店—長沙凱賓斯基酒店休息，並整理隔天會議所需資料與文件。

10月23日一大早起床用完早餐並打理完畢後，本人搭乘主辦單位精心安排的接駁車，經過20分鐘左右的車程抵達本次會議的開幕酒店—長沙洲際飯店，並至研討會櫃檯辦理會議註冊手續，在熟悉並參觀研討會各討論室地點與環境後，依循大會所提供的會議手冊資料，本人接著於上午九時15分參與研討會開幕儀式，儀式當中首先本次會議主席—福州大學 Artde Donald Kin-Tak Lam 教授致詞並宣讀歡迎辭，接著，由台灣知識創新學會會長—Teen-Hang Meen 教授致詞並頒發協辦本次研討會的國外與國內單位感謝狀，開幕式接下來即為與會來賓企盼，由大會特地邀請的主題演講(Keynote Speeches)。

首先第一場邀請主題演講為來自德州大學的 James P. Barufaldi 教授發表主題演講，演講題目是“Engineering as the Catalyst in STEM Education”，主要講述內容係說明如何藉由科學技術、工程、數理教育等訓練與催化，培育並增強學生與專家學者在科學與數學方面的認知技巧與活用能力，Barufaldi 教授以深入淺出的方式說明他在這方面教育的成果，並說明美式教育下的學生與專長人員的訓練方式，另本人對於未來培育國內技術與研發專才有更深入的啟發，以期培育人才與國際社會並駕齊驅；緊接著，大會安排目前任職於大仁科技大學校長且為成功大學講座教授的王駿發教授發表主題演講，王校長演講題目為“Organge Technology & Happiness Information”，主要講述聯合國目前所倡導之“World Happiness”與橘色科技(Orange Technology)的鏈結關係，王校長提到橘色科技的由來係導因於和諧的融合以及溫和的照顧，因此他發明了一個整合 H2O 模式、快樂的 3D 模式、See-H 以及 H-POS 工程演算法以及檢測、回饋快樂訊息資料庫的橘色科技技術，王教授生動且活潑的演講方式以及即席反應，深深擄獲與會嘉賓的目光並給予最熱烈的回饋，在王教授妙語如珠的結論中結束了早上的演講行程，最後，本人與所有與會專家學者合照留念。

當天下午本人與 Wang 教授共同擔任 Communication Science & Engineering 以及 Creative Media 領域(Session B2)的會議主席，該場次共有 “To Excavate the Determinants

of Mobile Communication Technology in Current Wireless Telecommunication Technology Era”、 “Progressive path selection scheme for mobile sink wireless sensor networks”、 “Box office Statistics analysis of Zhang Yi-Mou’ s Films in Spanish marketing ”、 “Primary Study of Attitudes of Schoolchildren in Rural and Remote Areas Toward Digital Imaging Learning-Take Film Making Summer Camp as an Example” 等 4 篇文章發表，內容大多講述如何利用智慧型網路工具以及大數據理論，處理不同 target 的方法與技術，並以理論模擬以及實際結果進行比對分析，獲得較佳的預期與定位結果，此間，本人亦前往海報會場張貼此次發表文章 “Origin of the electroluminescence from the annealed-ZnO/GaN heterojunction light-emitting diodes”，並與在長專家學者討論研究成果並交換研發心得，最後，參與大會精心安排的晚宴結束踏實而疲累的一天。

10 月 24 日經過舟車跋涉抵達下塌飯店鳳凰天下酒店後，除了在搭車期間與專家學者討論研究成果與心得外，亦聽取一些與研發相關的論文內容發表，其中，另人印象較深刻的是論文題目為 "Field Emission characteristics of ZnO Nanosheets nanostructure" 的研究成果，此研究係由 Young 教授帶領研究團隊利用水熱法於室溫條件下在矽基板上，沉積具有奈米片狀結構的氧化鋅材料，研究中除了探討不同製程條件下的奈米形貌與結晶特性外，更製作簡易元件，量測結構的場效增益值與導通電場，結果顯示，在氫氧化鈉濃度為 0.4M 時，元件的場效增益與導通電場分別為  $1014 \text{ V}/\mu\text{m}^2$  及  $5.04 \text{ V}/\mu\text{m}$ 。

10 月 25 日繼續停留在下塌的鳳凰天下酒店，經過兩天的適應認識更多傑出的專家學長，並獲得更多研發與研究的方法與技巧，在此期間對於一篇研究成果 “Visible Light Photocatalytic Study of Zinc Oxide Diode by Spray Pyrolysis” 特別感興趣，該文章係分別利用混成 indium nitrate 以及 bismuth nitrate 前驅物，以利用簡單的高溫熱解噴塗方式，於  $450^\circ\text{C}$  條件下製作 p 型與 n 型薄膜，藉由光電特性量測確認 p 型與 n 型氧化鋅特性，最終，利用 n 型、p 型以及 p-n 同質結構分別製作光感測元件，探討元件在可見光照射下的光觸媒活性，結果顯示，由於 p-n 同質結構具有較佳的內建電場可以有效分離光生電子-電洞對，因此具有最佳的光觸媒反應，該研究結果對於本人目前研發之氧化鋅同質界面二極體元件，提供相當有用的資訊與啟發，使本人對於刻正研發的內容預期成果更具信心。

10 月 26 日搭乘巴士抵達陽光酒店，稍事休息後與與會專家學長閒話家常，期間也看到另本人相當感興趣的研究成果，題目為 “Investigations on p-Si/i-ZnO/n-ZnO Heterojunction Photodetectors”，藉由比較與 p-Si/n-ZnO 光檢測器的電流-電壓操作結果，作者發現，元件的漏電流可以有效抑制，p-i-n 異質結構的整流特性可以達到  $6.64 \times 10^4$ ，該異質結構所製作之光檢測器元件，在紫外光波段(340 nm)照射下的感應電流增強 77 倍，而在可見光(500 nm)照射下的感應電流較 p-n 結構只增加 10 倍，因此，作者證明利用 p-i-n 異質結構所製作之光檢測器有較好的 UV-to-visible rejection ratio，此項結果，也與本人目前於製作 n-ZnO/p-GaN 異質界面發光二極體元件結果相呼應，對本人後續研究更增添信心。

10月27日搭乘巴士抵達下榻的京武鉑曼酒店會場，當天與其他領域學者套論研究成果與心得，於此期間發表的論文“Development and analysis of small size electrical field coupling wireless power system”令本人印象深刻，文章中提到製作小型無線傳輸電容器元建的可行性，作者利用三種電擊方式與結構製作出傳輸效率高達0.7的元件，且實際應用下的效率最高可達51%，而當電極面積為22.25 cm<sup>2</sup>時，無線傳輸的最大距離可達22.5 mm，雖然研究領域與本人不同，然而作者對於元件結構設計方法與技巧，則是提供本人對於現階段元件製作時的結構與電極製備時的啟發。

10月28日搭乘巴士回到研討會開幕時下榻的凱賓斯基酒店，期間與不同領域專家學者進行研討與意見交流，其中，由Zou教授發表“The Development of Indoor Positioning Aerial Robot Based on Motion Capture System”的文章，係採用四旋翼機進行室內空間的資訊捕捉，研究結果顯示，雖然在室外空間可以利用GPS定位系統準確操控旋翼機飛行，但在受限於GPS在室內空間的遮蔽效應，作者利用2.4 GHz的Xbee無線傳輸模式，以3D移動捕捉系統(3D motion capture system)可以使旋翼機準確偵測室內資訊，該項研究成果應用到感測技術與工具機，使本人對於目前政府極力推動之工業4.0政策，有更深入了解也更引起本人對於感測元件應用於工具機研究的興趣。

10月29日下午1點10，本人懷著依依不捨的心情，搭乘大會提供的巴士至長沙黃花國際機場搭乘華航班機飛抵台灣桃園國際機場。

## 心得及建議

本次參加在湖南湘潭所舉行的2015 International Conference on Innovation, Communication and Engineering國際研討會，除了有許多國外專家學者參加外，更有許多國內不同領域的知名學者與會，在開會期間除了可以與相關領域研究先進學習並討論研究成果外，藉由大會安排的各個專題與會議演講，更可以提供本人深入了解其他相關領域的研究內容與方向，提供本人進一步從事跨領域研究的動機與可行性，此外，大會精心安排的接送工具與行程，更可以讓本人在無後顧之憂的環境下，充分與與會學者專家先進進行深入的探討與學習，不僅有助於充實本人研究能量，更可以提供本人對於未來研究方向的啟發。

## 會議照片

大會開幕式：



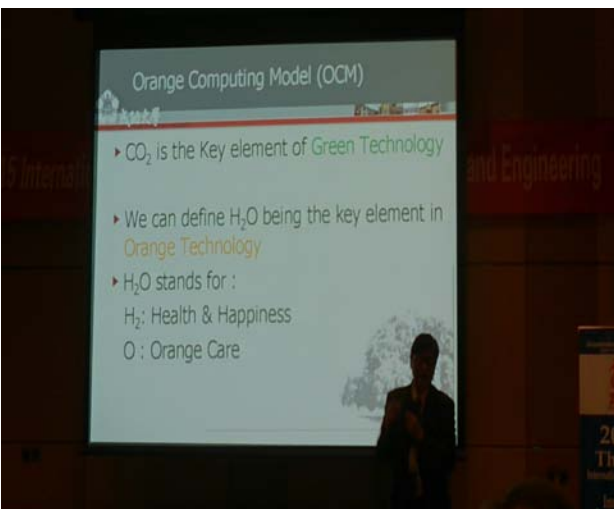
與發表論文海報合影



邀請演講內容：



研討會一隅



附錄：攜回資料名稱及封面

Proc. of 2015 The Fourth International Conference on Innovation, Communication and Engineering



**(A) Advanced Material Science & Engineering**

#1840

**Origin of the electroluminescence from the annealed-ZnO/GaN heterojunction light-emitting diodes**

Kai-Chiang Hsu<sup>1</sup>, Wei-Hua Hsiao<sup>1</sup>, Ching-Ting Lee<sup>2</sup>,  
Yan-Ting Chen<sup>1</sup> and Day-Shan Liu<sup>1</sup>

<sup>1</sup>Institute of Electro-Optical and Material Science, National Formosa University, Yunlin, Taiwan  
<sup>2</sup>Institute of Microelectronics, Department of Electrical Engineering, National Cheng Kung University, Tainan, Taiwan

**ABSTRACT:** This paper addressed the effect of a post-annealed treatment on the electroluminescence (EL) of an n-ZnO/p-GaN heterojunction light-emitting diode (LED). The bluish light emitted from the 450°C-annealed LED became reddish as the LED annealed at a temperature of 800°C under vacuum ambient. The origin of the evolutions on the light emission for these LEDs annealed at various temperatures was studied using the measurements of the electrical property, photoluminescence, and Auger electron spectroscopy (AES) depth profile. The blue-violet emission located at 430 nm associated with the intrinsic transitions of the n-ZnO and p-GaN layer, the green-yellow emission at 550 nm related to the defects transition of the native oxygen vacancies in the n-ZnO layer, and the red emission at 610 nm emerged from the Ga-O inlayer due to the interdiffusion between the n-ZnO/p-GaN interface were respectively responsible for the emission light of these annealed-LEDs. In addition, the above-mentioned mechanisms also supported the EL spectra of the LEDs annealed at 700°C under air, nitrogen, and oxygen ambient, respectively.

#1845

**Improvements of oil and conditioner to the hair keratin**

Chia-Ling Chang<sup>1</sup>, Tsung-Han Ho<sup>2</sup> and Te-Hua Fang<sup>3</sup>

<sup>1</sup>Department of Chemical and Materials Engineering, National Kaohsiung University of Applied Sciences, Kaohsiung 807, Taiwan & Min-Hwei Junior College of Health Care Management, Tainan 736, Taiwan

<sup>2</sup>Department of Chemical and Materials Engineering, National Kaohsiung University of Applied Sciences, Kaohsiung 807, Taiwan

<sup>3</sup>Department of Mechanical Engineering, National Kaohsiung University of Applied Sciences, Kaohsiung 807, Taiwan

**ABSTRACT:** In this study, we used atomic force microscopy and friction microscopy and Fourier transform infrared spectroscopy (FTIR) to detect the impact of hair products nourish hair phenomenon, and then compare the hair to repair the situation. We conducted experimental research on nourishing oils and hair conditioner, the findings osmotic absorption effect found hair milk is better. The surface roughness of the horny significantly is lower than the phenomenon of cuticle repair hair oil to good effect on wettability and softness of hair. FTIR was possible to observe wavenumber changes in the surface topography and interfacial structure after the hair damage and improvement. The local mechanical properties of the hair samples were discussed.

Article

# Origin of the Electroluminescence from Annealed-ZnO/GaN Heterojunction Light-Emitting Diodes

Kai-Chiang Hsu <sup>1</sup>, Wei-Hua Hsiao <sup>1</sup>, Ching-Ting Lee <sup>2</sup>, Yan-Ting Chen <sup>1</sup> and Day-Shan Liu <sup>1,\*</sup>

Received: 29 August 2015 ; Accepted: 9 November 2015 ; Published: 16 November 2015  
Academic Editor: Stephen D. Prior

<sup>1</sup> Institute of Electro-Optical and Materials Science, National Formosa University, Huwei, Yunlin 63201, Taiwan; 10376106@gm.nfu.edu.tw (K.-C.H.); s706802000213@gmail.com (W.-H.H.); a0922639175@gmail.com (Y.-T.C.)

<sup>2</sup> Institute of Microelectronics, Department of Electrical Engineering, National Cheng Kung University, Tainan 70101, Taiwan; ctlee@ee.ncku.edu.tw

\* Correspondence: dsliu@sunws.nfu.edu.tw; Tel.: +886-5-631-5665; Fax: +886-5-632-9257

**Abstract:** This paper addressed the effect of post-annealed treatment on the electroluminescence (EL) of an *n*-ZnO/*p*-GaN heterojunction light-emitting diode (LED). The bluish light emitted from the 450 °C-annealed LED became reddish as the LED annealed at a temperature of 800 °C under vacuum atmosphere. The origins of the light emission for these LEDs annealed at various temperatures were studied using measurements of electrical property, photoluminescence, and Auger electron spectroscopy (AES) depth profiles. A blue-violet emission located at 430 nm was associated with intrinsic transitions between the bandgap of *n*-ZnO and *p*-GaN, the green-yellow emission at 550 nm mainly originating from the deep-level transitions of native defects in the *n*-ZnO and *p*-GaN surfaces, and the red emission at 610 nm emerging from the Ga-O interlayer due to interdiffusion at the *n*-ZnO/*p*-GaN interface. The above-mentioned emissions also supported the EL spectra of LEDs annealed at 700 °C under air, nitrogen, and oxygen atmospheres, respectively.

**Keywords:** electroluminescence; *n*-ZnO/*p*-GaN heterojunction; light-emitting diode; photoluminescence; AES depth profile

## 1. Introduction

In recent decades, zinc oxide (ZnO) has attracted significant interest for short-wavelength optoelectronics applications for its wide and direct band gap ( $E_g \sim 3.37$  eV at 300 K) [1–3]. Furthermore, ZnO has advantages of excellent resistance to the radiation damage, suitable for the wet-etching process, and large exciton binding energy of 60 meV at room temperature; some ZnO-based optoelectronic applications are expected to be a good substitute for gallium nitride (GaN), another wide band gap ( $E_g \sim 3.4$  eV at 300 K) semiconductor that is the current state-of-the-art approach used for the production of green, blue-ultraviolet, and white light-emitting devices. ZnO has much simpler types of crystal-growth methods, such as sputtering, pulse laser deposition, and hydrothermal methods, resulting in cost-effective approaches for the production of ZnO-based devices [4–6]. Among these deposition methods, sputtering technology is a widely used technology for preparing quality and large-sized ZnO film on substrates at a relatively low temperature. However, although there has been some progress made using various growth methods and dopant elements to achieve *p*-ZnO [7–9], one current problem that impedes the development of ZnO-based homojunction devices is the lack of reliable and reproducible high quality *p*-type conductivity for ZnO. While *p*-ZnO is difficult to obtain, *p*-GaN which has an almost identical in-plane lattice parameter (lattice

mismatch ~1.8%) and wurtzite crystal structure to ZnO film, has been employed to realize an *n*–*p* heterojunction light emitting diode (LED). Such an LED is made by depositing *n*-ZnO onto the *p*-type GaN epilayer [10–13]. The luminescent property of *n*-ZnO is known to depend significantly on the crystal structure and content of various defects in the crystal. A short-wavelength band associated with the energy bandgap and a broad long-wavelength band including the involvement of zinc interstitial ( $Zn_i$ ), zinc vacancy ( $V_{Zn}$ ), oxygen vacancy ( $V_O$ ), and oxygen interstitial ( $O_i$ ) defects were generally observed from an undoped *n*-ZnO film [14–16]. To accomplish the aim of an *n*-ZnO/*p*-GaN heterojunction LED that emits pure short-wavelength radiation, it is necessary to address and engineer solutions to the above-mentioned visible emission that emerge from defects in *n*-ZnO film, as well as the radiation related to the *n*-ZnO/*p*-GaN interface and *p*-GaN epilayer. Lee *et al.*, studied the origin of *n*-ZnO/*p*-GaN heterojunction LEDs annealed under nitrogen and air atmospheres and they obtained a LED emitted blue light after a heterojunction structure was annealed under nitrogen atmosphere [17]. Recently, we also reported a LED that radiated only a near-UV emission when it was constructed from a 450 °C-annealed *n*-ZnO/*p*-GaN heterojunction structure under vacuum atmosphere [18]. Although researchers have endeavored to achieve LEDs that emit a short-wavelength light via thermal annealing of *n*-ZnO/*p*-GaN heterojunction structures, there are few reports that comprehensively discuss the origins of the device emission through the effect of various annealed processes on the heterojunction structures.

This study measured electroluminescence (EL) spectra as a function of *n*-ZnO/*p*-GaN heterojunction structures annealed at various temperatures and atmospheres. The origins responsible for the evolution of device radiation, that were prepared using *n*-ZnO/*p*-GaN heterojunction structures annealed at various temperatures under vacuum atmosphere, were elucidated with the help of the measurements of the electrical, optical, and material properties of the annealed *n*-ZnO film and an investigation of the annealed *n*-ZnO/*p*-GaN interface. The evolutions of the electrical and optical properties of *n*-ZnO films annealed at an elevated temperature under different atmospheres also were linked to the radiation properties of the resulting *n*-ZnO/*p*-GaN heterojunction LEDs.

## 2. Material Preparation and Experimental Procedure

An undoped ZnO (denoted as *n*-ZnO hereafter) film with a thickness of 100 nm was deposited onto an activated *p*-GaN:Mg epilayer with a hole concentration and carrier mobility of  $2.9 \times 10^{17} \text{ cm}^{-3}$  and  $15.5 \text{ cm}^2/\text{V}\cdot\text{s}$ , respectively, using a radio-frequency (RF) magnetron cosputtering system. A ZnO target (purity, 99.99%) with a diameter of 50 mm was sputtered at room temperature as the working pressure and rf power was adjusted to 1.33 Pa and 50 W, respectively, under a pure argon atmosphere. The pattern of the *n*-ZnO film on the *p*-GaN epilayer was defined using standard lift-off technology. In order to realize an *n*-ZnO/*p*-GaN heterojunction LED, it is important to obtain a quality ZnO film with sufficient carrier concentration. However, since the sputter-deposited *n*-ZnO film exhibited insulated behavior, a post-annealed treatment was employed to apply on the *n*-ZnO film to activate the native donors and to also facilitate crystallinity. Thus, the *n*-ZnO/*p*-GaN heterojunction structure was annealed in a furnace at temperatures ranging from 450 to 800 °C for 30 min under vacuum atmosphere. In addition, as-deposited *n*-ZnO/*p*-GaN heterojunction structures were also annealed under nitrogen, air, and oxygen atmospheres, respectively, at 700 °C for 30 min to provide a comparison to the luminescence property of a vacuum-annealed sample. The Ni/Au (5/50 nm) metal system was deposited onto a *p*-GaN surface and annealed at 500 °C for 10 min under air atmosphere to achieve ohmic contact behavior. Subsequently, a 150 nm-thick transparent indium tin oxide (ITO)-ZnO film [ $Zn / (Zn + In) = 33 \text{ at.}\%$ ] with an electron concentration and resistivity of  $5.3 \times 10^{20} \text{ cm}^{-3}$  and  $5.6 \times 10^{-4} \Omega\cdot\text{cm}$ , respectively, was deposited onto the patterned *n*-ZnO surface by a RF magnetron cosputtering system, using ZnO and ITO targets. The transparent ITO-ZnO electrode ohmic contact to the *n*-type ZnO was then optimized by a rapid thermal annealing (RTA) process at 400 °C for 5 min in vacuum atmosphere [18]. The contact behavior of the Au/Ni/*p*-GaN and ITO-ZnO/*n*-ZnO systems, respectively, was confirmed by using the transmission-line model

(TLM). The Au/Ni/*p*-GaN ohmic contact system exhibited a specific contact resistance of about  $10^{-2} \Omega \cdot \text{cm}^2$ , whereas all of the annealed *n*-ZnO contacted to the cosputtered ITO-ZnO electrode showed a specific contact resistance ranging from  $10^{-3}$  to  $10^{-4} \Omega \cdot \text{cm}^2$ . Generally, the EL spectrum from an *n-p* heterojunction LED was known to be composed of the radiation from the *n*- and *p*-side as well as the *n-p* interface. For the *n*-ZnO/*p*-GaN heterojunction LED, in order to extract the radiation emerging only from the *n*-ZnO film without interference from the *p*-GaN epilayer and diffusion at *n*-ZnO/*p*-GaN interface, the hall measurement, photoluminescence, XRD, and SEM data presented in this paper are conducted from the *n*-ZnO film deposited onto the silicon substrates and then annealed under the above-mentioned temperature and atmospheres.

Electrical properties including the carrier concentration, mobility, and resistivity of the annealed *n*-ZnO and cosputtered ITO-ZnO films as well as the activated *p*-GaN epilayer were measured using van der Pauw Hall measurements (Ecopia HMS-5000, Ecopia Anyang, South Korea) at room temperature. The radiative characteristics of the annealed *n*-ZnO films were determined from photoluminescence (PL) spectra measured at room temperature using a He-Cd laser ( $\lambda = 325 \text{ nm}$ ) pumping source. X-ray diffraction (XRD) patterns of the *n*-ZnO film annealed at various temperatures were obtained using a diffractometer (Siemens D-500, Siemens, Munich, Germany) with a Cu  $K\alpha$  radiation source. The corresponded surface morphologies of the annealed *n*-ZnO films were observed using a field emission scanning electron microscope (FE-SEM, JSM-6700F, JEOL, Tokyo, Japan) operated at 3 kV. The evolutions of the annealed *n*-ZnO/*p*-GaN interface were examined by Auger electron spectroscopy (AES) depth profile using a scanning Auger nanoprobe (ULVAC-PHI, PHI 700, ULVAC, Kanagawa, Japan). The current-voltage (I-V) properties of the LEDs fabricated by using annealed *n*-ZnO/*p*-GaN heterojunction structures as well as the ITO-ZnO/*n*-ZnO and Au/Ni/*p*-GaN ohmic contact systems were measured by a semiconductor parameter analyzer (HP4156C, Aglient, Santa Clara, CA, USA). The EL spectra of LEDs fabricated using annealed *n*-ZnO/*p*-GaN heterojunction structures were measured at room temperature under forward injection currents.

### 3. Results and Discussion

The electrical properties of *n*-ZnO films annealed at 450, 500, 600, 700, and 800 °C, respectively, under vacuum atmosphere for 30 min are summarized in Table 1. All these films exhibited *n*-type conduction with electron carriers higher than  $10^{18} \text{ cm}^{-3}$ , indicating that large amounts of native donors were activated after the films were annealed under vacuum atmosphere. Carrier concentration and hall mobility both increased with increasing annealing temperature and then decreased as the annealed temperature reached 800 °C. The largest electron concentration of  $2.4 \times 10^{19} \text{ cm}^{-3}$  and the highest carrier mobility of  $16.2 \text{ cm}^2/\text{V} \cdot \text{s}$  were concurrently found from *n*-ZnO annealed at 700 °C under vacuum atmosphere for 30 min. Figure 1 shows the room temperature PL spectra (RTPL) of the as-deposited *n*-ZnO film and the films annealed at various temperatures. Since the sputter-deposited *n*-ZnO film was abundant in non-radiative defects, the emission intensity was too weak to be observed. For the as-deposited film annealed under vacuum atmosphere, two distinct peaks located at near UV (~380 nm) and green (~550 nm) wavelengths were observed from the associated PL spectra. The peak at the short wavelength was denoted as a near-band-edge (NBE) emission that was related to the transition from the energy bandgap of ZnO, whereas the broad emission around the visible wavelengths emerged from the deep-level (DL) emission composed of native defects of  $V_{\text{Zn}}$ ,  $\text{Zn}_i$ , and  $V_{\text{O}}$  in the annealed *n*-ZnO film [19,20]. Since atoms at the *n*-ZnO film surface, especially for the oxygen atoms, were in favor of outdiffusion when the film was annealed under vacuum atmosphere at an elevated temperature [21], the peak of the DL emission was close to the peak related to the  $V_{\text{O}}$  transition, reported at about 580 nm [22]. The slight blue-shift of the DL emission as the annealed temperature increased could be ascribed to the increase in the  $V_{\text{Zn}}$ -related transitions [21]. In addition, both the emission intensity of the NBE and DL were enhanced when the annealed temperature increased as the post-annealed process was favorable

for the radiation recombination originating from the improvement in the crystalline structure. This was especially the case for samples annealed at a temperature higher than 600 °C. Therefore, carrier concentrations that were mainly linked to the activation of  $V_O$  donors and Hall mobility associated with crystallinity increased as the  $n$ -ZnO film annealed at temperatures increased from 450 to 700 °C, as shown in Table 1. However, although the NBE emission in the PL spectrum of the  $n$ -ZnO film annealed at 800 °C was significantly increased as compared to the DL emission, Hall mobility was lower than in film annealed at 700 °C, implying structural degradation when the  $n$ -ZnO film annealed at this temperature. XRD patterns of the  $n$ -ZnO films annealed at 450, 700, and 800 °C, respectively, under vacuum atmosphere for 30 min are shown in Figure 2a. All of these  $n$ -ZnO films exhibited a hexagonal wurtzite structure with a  $c$ -axis ZnO (002) growth orientation preference. The evidence of crystallinity as a consequence of the  $n$ -ZnO film being annealed at a temperature of the 700 °C was seen from the decrease in the full width at half maximum (FWHM) of ZnO (002) in these XRD diffraction patterns. The corresponding crystal size of  $n$ -ZnO films annealed at 450 and 700 °C, using the Debye-Scherer formula, was about 21.9 and 34.7 nm, respectively. In addition, as quoted from report [23], the shift of the ZnO (002) peak toward a high diffraction angle as compared to bulk ZnO ( $2\theta = 34.42^\circ$ ) was ascribed to the reduction in the  $c$ -axis lattice constant due to the formation of  $V_O$  defects for the sample annealed under vacuum atmosphere. Interestingly, although the  $n$ -ZnO film annealed at 800 °C exhibited the most intense radiation emission, its crystal size apparently shrunk to 17.3 nm, indicating degradation of the crystalline structure. Figure 2b,c shows the surface morphologies of the  $n$ -ZnO film annealed at 700 °C, and 800 °C, respectively. The surface morphology of the  $n$ -ZnO film annealed at 700 °C (Figure 2b) was textured with obvious crystal grains. In contrast, the degradation in the crystalline structure of the sample annealed at 800 °C exhibited a surface feature of ambiguous crystal grains. Moreover, the appearance of the porous features as indicated by arrows in Figure 2c was attributed to an excess outdiffusion of the atoms from the surface of the  $n$ -ZnO film. The increase in grain boundaries was a consequence of the reduction in crystal size and the formation of a porous structure. The grain boundaries obstructed carrier transition, and thereby resulted in the decrease of Hall mobility as listed in Table 1. Accordingly, these films annealed under vacuum atmosphere were both favorable for the growth of crystal size and for enhancement of radiation emission, especially for  $V_O$ -related emission. However, degradation in the crystalline structure and apparent reduction in the crystal size was observed from the sample annealed at 800 °C, where there was a distinct outdiffusion of surface atoms. Furthermore, in terms of the film's luminescence, the apparent shrinkage in crystal size obtained from the 800 °C-annealed  $n$ -ZnO film might promote recombination of photo-generated electron-hole pairs due to the size-confinement effect, and therefore the emission intensity increased accordingly [24,25].

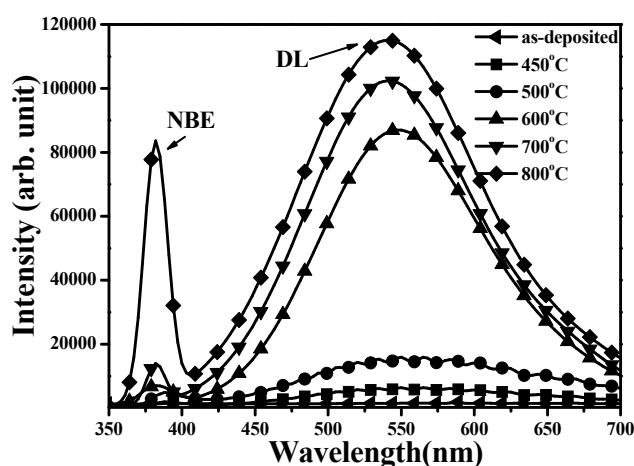


**Figure 1.** Room temperature photoluminescence (RTPL) spectra of as-deposited  $n$ -ZnO film and the films annealed at 450, 500, 600, 700, and 800 °C, respectively, under vacuum atmosphere for 30 min.

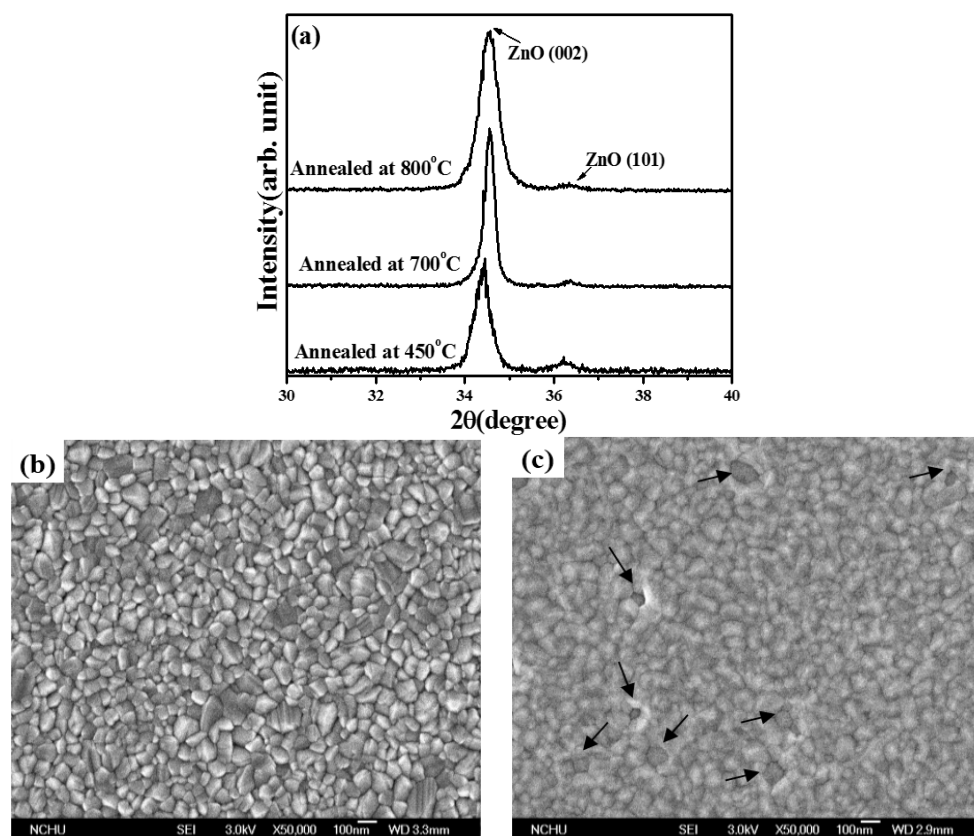


**Figure 2.** (a) X-ray diffraction (XRD) patterns of *n*-ZnO films annealed at 450, 700, and 800 °C, respectively, under vacuum atmosphere for 30 min and surface morphologies of (b) 700 °C- and (c) 800 °C-annealed *n*-ZnO films.

**Table 1.** Electrical properties of *n*-ZnO films annealed at 450, 500, 600, 700, and 800 °C, respectively, under vacuum atmosphere for 30 min.

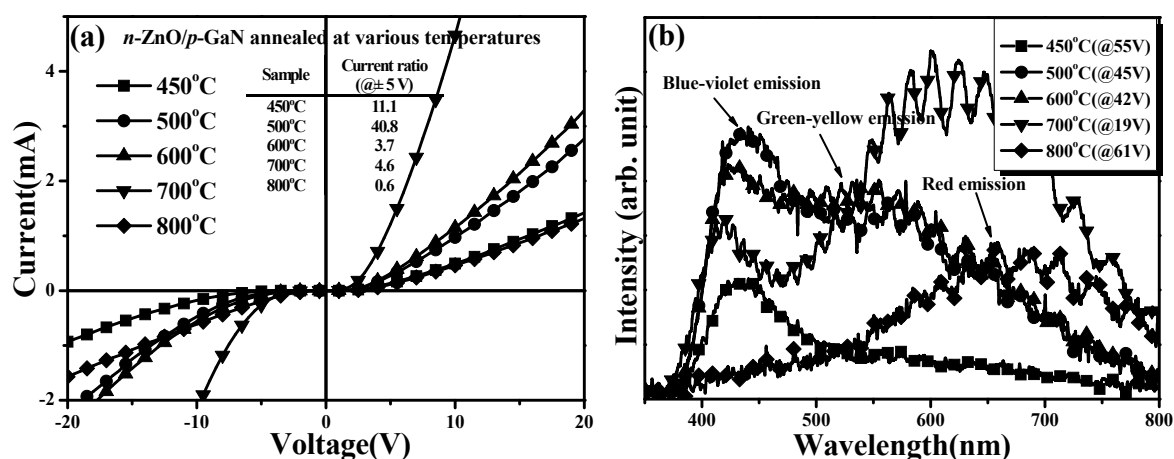
Annealed Temperature	$n$ (cm <sup>-3</sup> )	$\mu$ (cm <sup>2</sup> /V·s)	$\rho$ (Ω·cm)
450 °C	$-1.2 \times 10^{18}$	3.0	3.1
500 °C	$-7.3 \times 10^{18}$	7.3	$1.2 \times 10^{-1}$
600 °C	$-1.6 \times 10^{19}$	9.4	$4.3 \times 10^{-2}$
700 °C	$-2.4 \times 10^{19}$	16.2	$1.6 \times 10^{-2}$
800 °C	$-1.7 \times 10^{19}$	12.4	$2.4 \times 10^{-2}$

The I-V characteristics of diodes fabricated using *n*-ZnO/*p*-GaN heterojunction structures annealed at temperatures of 450, 500, 600, 700, and 800 °C, respectively, under vacuum atmosphere for 30 min, are shown in Figure 3a. All these diodes exhibited nonlinear behavior with different series resistances and turn-on voltages. Series resistance and turn-on voltage were optimized to 1.65 kΩ and 2.52 V, respectively, for the *n*-ZnO/*p*-GaN heterojunction structure annealed at 700 °C. This was done because the 700 °C-annealed *n*-ZnO film had the lowest resistivity of  $1.6 \times 10^{-2}$  Ω·cm and the ITO-ZnO/*n*-ZnO ohmic contact system also exhibited the best contact resistance of  $2.9 \times 10^{-4}$  Ω cm<sup>2</sup>. Degradation in the crystalline structure and increase in film resistivity of the 800 °C-annealed *n*-ZnO film resulted in a diode that performed with a high turn-on voltage of 3.24 V and a very high series resistance. The apparent decrease in the current ratio of the 800 °C-annealed sample, measured from the forward turn-on current to reverse leakage current, as shown in the inset table, also implied that there was degradation of the *n*-ZnO/*p*-GaN interface.

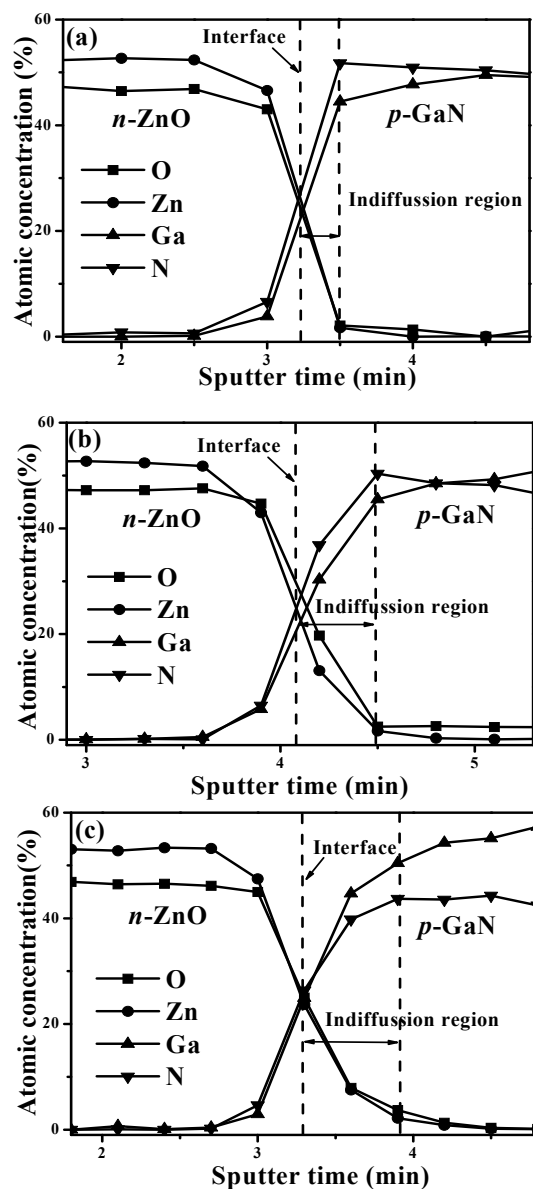
Figure 3b presents the EL spectra of annealed  $n$ -ZnO/ $p$ -GaN heterojunction LEDs as a function of the annealed temperatures, measured under an injection current of 20 mA. Only one distinct peak at about 430 nm (denoted as a blue-violet emission in the figure) with a tail extending to the long-wavelengths was obtained from the LED using the 450 °C-annealed  $n$ -ZnO/ $p$ -GaN heterojunction structure. For the heterojunction structure annealed at 500 °C, the blue-violet emission was obviously enhanced and another broad peak at about 550 nm (denoted as a green-yellow emission in the figure) appeared in the EL spectrum. The relative intensity of the green-yellow emission from the LED constructed from the 600 °C-annealed  $n$ -ZnO/ $p$ -GaN heterojunction structure was almost comparable to that of the blue-violet emission. When the  $n$ -ZnO/ $p$ -GaN heterojunction structure was annealed at 700 °C, a broad and intense emission located approximately at 620 nm (denoted as a red emission), became the dominant radiation. However, only one broad and weak emission at about 650 nm, with an ambiguous tail extending to the short-wavelengths, was observed from the LED fabricated using the 800 °C-annealed  $n$ -ZnO/ $p$ -GaN heterojunction structure. In general, the electroluminescence of a traditional  $p$ - $n$  heterojunction LED was a factor in the structural quality of the active region and the evolution of the interface. Accordingly, these EL spectra were mainly composed of the radiation from the  $p$ -GaN side and only a little portion of the emission from the  $n$ -ZnO side, since the active region of these  $n$ -ZnO/ $p$ -GaN heterojunction LEDs was mostly on the  $p$ -GaN side as conducted from the carrier concentration of  $n$ -ZnO and  $p$ -GaN layer. As quoted from reports [17,18,26–28], blue-violet emission was attributed to intrinsic transitions of  $n$ -ZnO film (NBE transition  $\sim$ 393 nm) and  $p$ -GaN epilayer (shallow donor to the deep Mg-acceptor level transition  $\sim$ 433 nm), as well as the interfacial recombination ( $\sim$ 410 nm), whereas green-yellow emission was linked to deep-level defect transitions, such as the  $V_O$  in the  $n$ -ZnO and gallium vacancy-related defects ( $V_{Ga}$ ) in the  $p$ -GaN layers, respectively. In addition, red emission was related to the emission of the Ga–O interlayer originating from the excess oxygen atoms diffused into to the  $p$ -GaN surface [17,27,29,30]. The peak of the blue-violet emission ( $\sim$ 430 nm) from the 450 °C-annealed LED was very close to the radiation from intrinsic transition of the  $p$ -GaN epilayer as a consequence of the dominant carriers recombination appearing on the  $p$ -GaN side. The blue-violet emission from the 500 °C-annealed sample was enhanced due to the increase in the annealed temperature and was demonstrated as facilitating the crystallinity of the  $n$ -ZnO film, which might be in favor of the electron carriers injection as compared to the 450 °C-annealed  $n$ -ZnO film. Furthermore, this LED also radiated a broad and significant long-green-yellow emission, although the green-yellow emission associated with the  $V_{Ga}$ -related defects was absent in the  $p$ -GaN conductive layer [28], indicating that the surface of the  $p$ -GaN epilayer was damaged with the formation of deep-level defects. Since the vacuum-annealed process was demonstrated to be favorable for the outdiffusion of the oxygen atoms at  $n$ -ZnO surface, these energetic oxygen atoms at the  $p$ -GaN surface would greatly enhance the formation of both the  $V_{Ga}$  and  $O_N$  defects at the  $p$ -GaN surface, which hardly appeared in the  $p$ -GaN conductive layer. Accordingly, the green-yellow emission associated with the  $V_{Ga}$ - $O_N$  transition was observed from the resulting LED [31–34]. The noteworthy red emission observed from the LED fabricated using a 700 °C-annealed  $n$ -ZnO/ $p$ -GaN heterojunction structure was evidence of the formation of the Ga–O interlayer originating from the oxygen atoms that indiffused into the  $p$ -GaN surface. Although the single  $n$ -ZnO film annealed at 700 °C under vacuum atmosphere exhibited the best structural quality as described earlier, the outdiffusion of the oxygen atoms at the  $n$ -ZnO surface led to degradation of the  $n$ -ZnO/ $p$ -GaN interface due to formation of a Ga–O interlayer.

The surface of the  $p$ -GaN damaged by the oxygen atoms indiffusion led to a decrease in the intrinsic emission from  $p$ -GaN, and thereby the peak of the blue-violet emission was blue-shifted toward 420 nm which was closer to radiation from interfacial recombination rather than from intrinsic emission from  $p$ -GaN. In addition, degradation in the crystalline structure due to excessive outdiffusion of atoms in the  $n$ -ZnO film and enhancement in the formation of the Ga–O interlayer at the  $p$ -GaN surface might be responsible for the significant decrease in device emission as observed from the 800 °C-annealed LED. The AES depth profiles of the  $n$ -ZnO/ $p$ -GaN heterojunction structures

annealed at 450 °C, 700 °C, and 800 °C shown in Figure 4a–c, respectively, are presented to study the evolution of the *n*-ZnO/*p*-GaN interface and the origin of the distinct degradation in the intensity of the electroluminescence for LED fabricated using the 800 °C-annealed sample. In these figures, the *n*-ZnO/*p*-GaN interface is determined at half of the Zn atoms as compared to the bulk *n*-ZnO film, while the indiffusion region is denoted as the region from the interface to the saturation of the oxygen atoms in the *p*-GaN epilayer. The atoms in the 700 °C- and 800 °C-annealed samples showed apparent interdiffusion at the *n*-ZnO/*p*-GaN interface as compared to the 450 °C-annealed samples. The indiffusion region that appeared in the *n*-ZnO/*p*-GaN heterojunction structure annealed at 800 °C, which was related to the O and Zn atoms from the *n*-ZnO surface to the *p*-GaN side, was significantly wider than that of the 700 °C-annealed sample. The formation of the Ga-O interlayer originating from the indiffusion of the O atoms at the *p*-GaN side was responsible for the resulting electroluminescence of the LED device being dominated by the red luminescence. In addition, the atomic concentration of N at the *p*-GaN side adjacent to the indiffusion region in the 800 °C-annealed sample (~43%) was markedly lower than the concentration of the Ga (~50.43%), whereas those of the N in the 450 °C- and 700 °C-annealed sample were about 51.7% and 50.3%, respectively, indicating that severe degradation of the *p*-GaN surface had occurred as it was annealed at 800 °C. Since an insufficient number of N atoms was favorable for the increase of the  $V_N$  donors, the hole carrier concentration at the *p*-GaN surface was thus reduced, and thereby led to significant degradation in the electrical and optical performance of the resulting LED device. Accordingly, although the annealed process on the *n*-ZnO/*p*-GaN heterojunction structures at an elevated temperature under vacuum atmosphere was favorable for enhancing the electroluminescence intensity of the resulting LED, blue-green and greenish light, respectively, was emitted from the 500 °C- and 600 °C-annealed LEDs due to the appearance and enhancement of the green-yellow emission which was related to deep-level defect transitions. By contrast, red emission emerging from the Ga-O interlayer due to indiffusion of oxygen atoms to *p*-GaN became the dominating emission for LED fabricated using 700 °C-annealed *n*-ZnO/*p*-GaN heterojunction structures resulting in the device emitting orange-yellow light. Moreover, significant indiffusion of Zn and O atoms from the *n*-ZnO surface to the *p*-GaN side and degradation in the *p*-GaN layer for the sample annealed at 800 °C weakened the electroluminescence intensity of the resulting LED and thus the device emitted a reddish light.



**Figure 3.** (a) Current-voltage (I-V) characteristics of diodes fabricated using *n*-ZnO/*p*-GaN heterojunction structures annealed at temperatures of 450, 500, 600, 700, and 800 °C, respectively, under vacuum atmosphere for 30 min and (b) electroluminescence (EL) spectra of these diodes measured under an injection current of 20 mA.



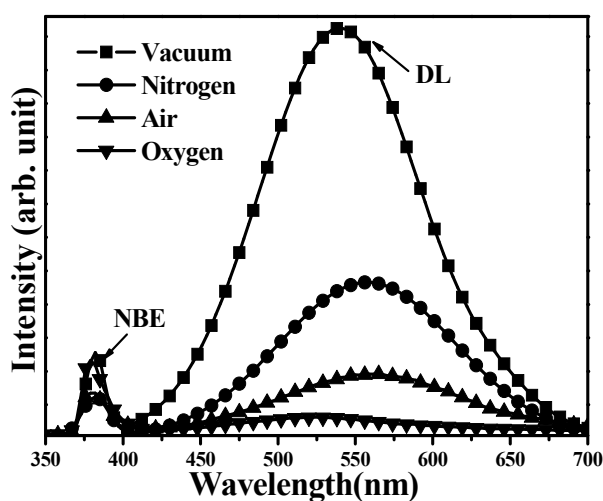
**Figure 4.** Auger electron spectroscopy (AES) depth profiles of *n*-ZnO/*p*-GaN heterojunction structures annealed at (a) 450 °C; (b) 700 °C and (c) 800 °C, respectively, under vacuum atmosphere for 30 min.

Table 2 summarizes the electrical properties of *n*-ZnO films annealed at 700 °C under nitrogen, air, and oxygen atmospheres, respectively (the sample annealed under vacuum atmosphere is also given for comparison). The RTPL spectra of the *n*-ZnO film annealed under various atmospheres at 700 °C for 30 min are presented in Figure 5. The activated electrons in the *n*-ZnO films were suppressed when these gases were introduced into the post-annealed atmosphere. The decrease in the electron carriers also led to the apparent reduction in the DL emission that mainly emerged from the  $V_O$ -related transition as described earlier. Since *n*-ZnO film annealed under the atmosphere incorporating the oxygen atoms was also beneficial for compensation of  $V_O$  defects [35], the  $V_O$ -related radiation was decreased more effectively for the sample annealed under air atmosphere, and it was almost absent in the RTPL spectrum of the oxygen-annealed *n*-ZnO film. Meanwhile, the electron concentration in *n*-ZnO film annealed under oxygen atmosphere was also minimized to  $2.7 \times 10^{17} \text{ cm}^{-3}$ , which was two orders of magnitude lower than the sample annealed under vacuum atmosphere. However, although the  $V_O$ -related defects were compensated by introducing

an additive gas during the post-annealed treatment, the crystalline structures of the *n*-ZnO films were thought to be inferior to the sample annealed under vacuum atmosphere as evidence of the marked decrease in carrier mobility. As mentioned in reports [36,37], such degradation in crystalline structure was ascribed to the compression of the crystal size due to the incorporation of ambient atoms in the film surface during thermal annealing, thereby resulting in an increase of the grain boundaries for carrier scattering causing the reduction in the carrier mobility. *I*-*V* curves of diodes fabricated using *n*-ZnO/*p*-GaN heterojunction structures annealed at 700 °C under vacuum, nitrogen, air, and oxygen atmospheres, respectively, for 30 min are shown in Figure 6a. Turn-on currents of each diode were strongly correlated with the resistivity of these annealed *n*-ZnO films, as listed in Table 2. The higher the resistivity of the *n*-ZnO film, the smaller the turn-on current measured. Figure 6b shows the EL spectra of these LEDs as a function of *n*-ZnO/*p*-GaN heterojunction structures annealed under various atmospheres. The EL spectra of the vacuum-, nitrogen-, and air-annealed LEDs were measured under an injection current of 20 mA, while that of the oxygen-annealed LED was obtained under an injection current of 10 mA. The radiation efficiency of these LEDs fabricated using the *n*-ZnO/*p*-GaN heterojunction structures annealed under nitrogen, air, and oxygen atmospheres, respectively, was inferior to the vacuum-annealed sample. The degradation in device electroluminescence was attributed to their large series resistance and the poor crystalline structure in the *n*-ZnO film. Figure 6b also shows that the relative intensity of the red emission that emerged from the Ga-O interlayer due to the oxygen atoms in the *n*-ZnO surface diffused into the *p*-GaN side was gradually reduced when the annealed atmosphere on *n*-ZnO/*p*-GaN heterojunction structures was incorporated with oxygen gas. A LED emitting bluish light with an absence of red emission was thus achievable when it was fabricated using an *n*-ZnO/*p*-GaN heterojunction structure annealed under oxygen atmosphere.

**Table 2.** Electrical properties of *n*-ZnO films annealed at 700 °C under vacuum, nitrogen, air, and oxygen atmospheres, respectively, for 30 min.

Annealed Atmosphere	$n$ (cm <sup>-3</sup> )	$\mu$ (cm <sup>2</sup> /V s)	$\rho$ ( $\Omega$ cm)
Vacuum	$-2.4 \times 10^{19}$	16.2	$1.6 \times 10^{-2}$
Nitrogen	$-1.7 \times 10^{18}$	3.9	$9.3 \times 10^{-1}$
Air	$-1.2 \times 10^{18}$	2.9	3.2
Oxygen	$-2.7 \times 10^{17}$	1.6	7.9



**Figure 5.** Room temperature PL spectra of *n*-ZnO films annealed at 700 °C under vacuum, nitrogen, air, and oxygen atmospheres, respectively, for 30 min.

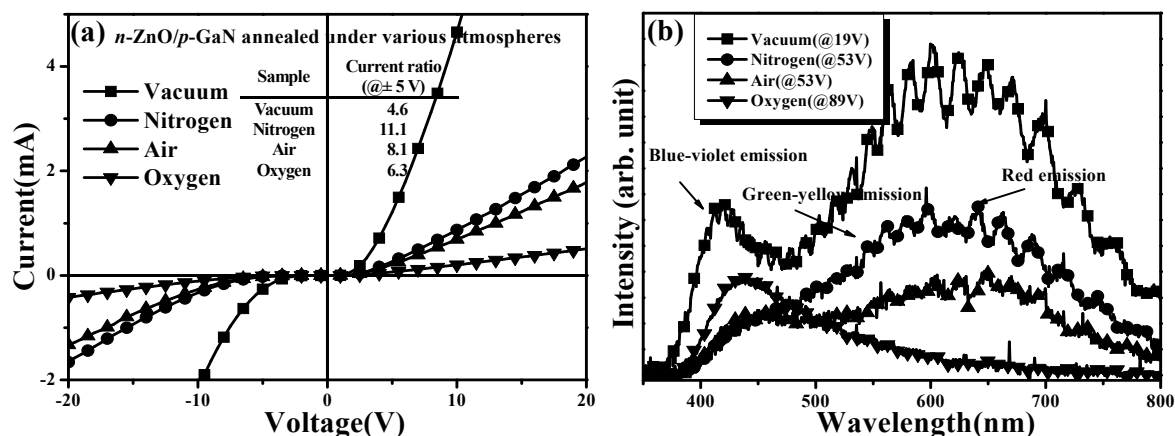


**Figure 6.** (a) I-V characteristics of diodes fabricated using *n*-ZnO/*p*-GaN heterojunction structures annealed under vacuum, nitrogen, air, and oxygen atmospheres, respectively, at 700 °C for 30 min and (b) EL spectra of these diodes measured under forward injection current.

#### 4. Conclusions

The origin of electroluminescence from annealed *n*-ZnO/*p*-GaN heterojunction diodes was elucidated with the help of an investigation of the electrical, optical, and material properties of annealed *n*-ZnO films and elemental distribution at the *n*-ZnO/*p*-GaN interface. LED fabricated using an *n*-ZnO/*p*-GaN heterojunction structure annealed at 450 °C under vacuum atmosphere radiated bluish light that was ascribed to blue-violet emission associated with the intrinsic transitions of *n*-ZnO film and *p*-GaN epilayer dominating over the EL spectrum. Although radiation was significantly improved from LEDs constructed from *n*-ZnO/*p*-GaN heterojunction structures that were annealed at temperatures higher than 450 °C, the promotion of deep-level transitions in the *n*-ZnO and *p*-GaN layers, respectively, resulted in an apparent enhancement of green-yellow emission, and as such, 500 °C- and 600 °C-annealed LEDs emitted greenish light. In addition, radiation from LED fabricated using a 700 °C-annealed *n*-ZnO/*p*-GaN heterojunction structure became yellowish as a consequence of the dominating red emission related to the formation of a Ga-O interlayer at the *n*-ZnO/*p*-GaN interface. For an *n*-ZnO/*p*-GaN heterojunction structure annealed at 800 °C, the resulting LED radiated a weak and broad red emission with blue-violet and green-yellow emissions being almost absent due to degradation in both the *n*-ZnO and *p*-GaN surfaces which was confirmed by the crystalline structure of the *n*-ZnO film and the elemental distribution at the *n*-ZnO/*p*-GaN interface. For *n*-ZnO films annealed at 700 °C under nitrogen and air atmospheres, although the formation of  $V_O$ -related defects was effectively suppressed as compared to the vacuum-annealed sample, growth of the crystalline structure was limited. Thus the radiation of the resulting LEDs was obviously inferior to LED constructed from an *n*-ZnO/*p*-GaN heterojunction structure annealed under vacuum atmosphere. Moreover, red and green-yellow emissions related to the oxygen atoms out-diffused from the *n*-ZnO surface to the *p*-GaN side were markedly depressed as the annealed atmosphere incorporated oxygen atoms. LED that radiated almost a blue-violet emission was achievable from an *n*-ZnO/*p*-GaN heterojunction structure annealed at 700 °C under an oxygen atmosphere.

**Acknowledgments:** This work was supported by Ministry of Science and Technology under MOST 103-2221-E-150-024 and ITRI South under B200-104AE2.

**Author Contributions:** Day-Shan Liu organized and designed the experiment procedures; Ching-Ting Lee supported the measurements and wrote this paper; Kai-Chiang Hsu, Wei-Hua Hsiao and Yan-Ting Chen executed the film deposition, measurements and resulting device analysis. All authors read and approved the final version of the manuscript to be submitted.

**Conflicts of Interest:** The authors declare no conflict of interest.

## References

1. Liu, K.; Sakurai, M.; Aono, M. Review: ZnO-based ultraviolet photodetectors. *Sensors* **2010**, *10*, 8604–8634. [[CrossRef](#)] [[PubMed](#)]
2. Lu, T.C.; Lai, Y.Y.; Lan, Y.P.; Huang, S.W.; Chen, J.R.; Wu, Y.C.; Hsieh, W.F.; Deng, H. Room temperature polariton lasing *vs.* photon lasing in a ZnO-based hybrid microcavity. *Opt. Express* **2012**, *20*, 5530–5537. [[CrossRef](#)] [[PubMed](#)]
3. Wang, L.; Kang, Y.; Liu, X.; Zhang, S.; Huang, W.; Wang, S. ZnO nanorod gas sensor for ethanol detection. *Sens. Actuator B-Chem.* **2012**, *162*, 237–243. [[CrossRef](#)]
4. Ibupoto, Z.H.; Khun, K.; Eriksson, M.; AlSalhi, M.; Atif, M.; Ansari, A.; Willander, M. Hydrothermal growth of vertically aligned ZnO nanorods using a biocomposite seed layer of ZnO nanoparticles. *Materials* **2015**, *6*, 3584–3597. [[CrossRef](#)]
5. Chang, R.H.; Yang, K.C.; Chen, T.H.; Lai, L.W.; Lee, T.H.; Yao, S.L.; Liu, D.S. Surface modification on the sputtering-deposited ZnO layer for ZnO-based Schottky diode. *J. Nanomater.* **2013**, *2013*. [[CrossRef](#)]
6. Ko, K.Y.; Kang, H.; Park, J.; Min, B.; Lee, H.S.; Im, S.; Kang, J.Y.; Myoung, J.; Jung, J.; Kim, S.; *et al.* ZnO homojunction core-shell nanorods ultraviolet photo-detecting diodes prepared by atomic layer deposition. *Sens. Actuator A Phys.* **2014**, *210*, 197–204. [[CrossRef](#)]
7. Zhao, J.Z.; Liang, H.W.; Sun, J.C.; Bian, J.M.; Feng, Q.J.; Hu, L.Z.; Zhang, H.Q.; Liang, X.P.; Luo, Y.M.; Du, G.T. Electroluminescence from n-ZnO/p-ZnO: Sb homojunction light emitting diode on sapphire substrate with metal-organic precursors doped p-type ZnO layer grown by MOCVD technology. *J. Phys. D Appl. Phys.* **2008**, *41*. [[CrossRef](#)]
8. Yang, T.H.; Wu, J.M. Thermal stability of sol-gel p-type Al-N codoped ZnO films and electric properties of nanostructured ZnO homojunctions fabricated by spin-coating them on ZnO nanorods. *Acta Mater.* **2012**, *60*, 3310–3320. [[CrossRef](#)]
9. Chiou, H.R.; Chen, T.H.; Lai, L.W.; Lee, C.T.; Hong, J.D.; Liu, D.S. The achievement of a zinc oxide-based homo-junction diode using radio frequency magnetron cosputtering system. *J. Nanomater.* **2015**, *2015*. [[CrossRef](#)]
10. Dalui, S.; Lin, C.C.; Lee, H.Y.; Yen, S.F.; Lee, Y.J.; Lee, C.T. Electroluminescence from solution grown n-ZnO Nanorod/p-GaN-heterostructured light emitting diodes. *J. Electrochem. Soc.* **2010**, *157*, H516–H518. [[CrossRef](#)]
11. Xu, S.; Xu, C.; Liu, Y.; Hu, Y.; Yang, R.; Yang, Q.; Ryou, J.H.; Kim, H.J.; Lochner, Z.; Choi, S.; *et al.* Ordered nanowire array blue/near-UV light emitting diodes. *Adv. Mater.* **2010**, *22*, 4749–4753. [[CrossRef](#)] [[PubMed](#)]
12. Goh, E.S.M.; Yang, H.Y.; Chen, T.P.; Ostrikov, K. Controlled electroluminescence of n-ZnMgO/p-GaN light-emitting diodes. *Appl. Phys. Lett.* **2012**, *101*. [[CrossRef](#)]
13. Mo, X.; Fang, G.; Long, H.; Li, S.; Huang, H.; Wang, H.; Liu, Y.; Meng, X.; Zhang, Y.; Pan, C. Near-ultraviolet light-emitting diodes realized from n-ZnO nanorod/p-GaN direct-bonding heterostructures. *J. Lumin.* **2013**, *137*, 116–120. [[CrossRef](#)]
14. Wang, Y.G.; Lau, S.P.; Lee, H.W.; Yu, S.F.; Tay, B.K.; Zhang, X.H.; Hng, H.H. Photoluminescence study of ZnO films prepared by thermal oxidation of Zn metallic films in air. *J. Appl. Phys. Lett.* **2003**, *94*, 354–358. [[CrossRef](#)]
15. Özgür, U.; Alivov, Y.I.; Liu, C.; Teke, A.; Reshchikov, M.A.; Doian, S.; Avrutin, V.; Cho, S.J.; Morkoç, H. A comprehensive review of ZnO materials and devices. *J. Appl. Phys.* **2005**, *98*. [[CrossRef](#)]
16. Willander, W.; Nur, O.; Sadaf, J.R.; Qadir, M.I.; Zaman, S.; Zainelabdin, A.; Bano, N.; Hussain, I. Luminescence from zinc oxide nanostructures and polymers and their hybrid devices. *Materials* **2010**, *3*, 2643–2667. [[CrossRef](#)]
17. Lee, J.Y.; Lee, J.H.; Kim, H.S.; Lee, C.H.; Ahn, H.S.; Cho, H.K.; Kim, Y.Y.; Kong, B.H.; Lee, H.S. A study on the origin of emission of the annealed n-ZnO/p-GaN heterostructure LED. *Thin Solid Films* **2009**, *517*, 5157–5160. [[CrossRef](#)]
18. Ho, C.C.; Lai, L.W.; Lee, C.T.; Yang, K.C.; Lai, B.T.; Liu, D.S. Transparent cosputtered ITO-ZnO electrode ohmic contact to n-type ZnO for ZnO/GaN heterojunction light-emitting diode. *J. Phys. D Appl. Phys.* **2013**, *46*. [[CrossRef](#)]
19. Shi, L.B.; Jin, J.W.; Xu, C.Y. A study on the magnetic properties in nitrogen-doped ZnO using first principles. *Mod. Phy. Lett. B* **2010**, *24*, 2171–2186. [[CrossRef](#)]

20. Rodnyi, P.A.; Khodyuk, I.V. Optical and luminescence properties of zinc oxide. *Opt. Spectrosc.* **2011**, *111*, 776–785. [CrossRef]
21. Yao, S.L.; Hong, J.D.; Lee, C.T.; Ho, C.Y.; Liu, D.S. Determination of activation behavior in the annealed Al–N Codoped ZnO Films. *J. Appl. Phys.* **2011**, *109*. [CrossRef]
22. Morkoç, H.; ÖZgür, U. *Zinc Oxide: Fundamentals, Materials and Device Technology*; Wiley-VCH: Weinheim, Germany, 2009.
23. Li, X.; Wang, Y.; Liu, W.; Jiang, G.; Zhu, C. Study of oxygen vacancies' influence on the lattice parameter in ZnO thin film. *Mater. Lett.* **2012**, *85*, 25–28. [CrossRef]
24. Cheng, H.M.; Lin, K.F.; Hsu, H.C.; Hsieh, W.F. Size dependence of photoluminescence and resonant Raman scattering from ZnO quantum dots. *Appl. Phys. Lett.* **2006**, *88*. [CrossRef]
25. Hu, S.Y.; Lee, Y.C.; Lee, J.W.; Huang, J.C.; Shen, J.L.; Water, W. The structural and optical properties of ZnO/Si thin films by RTA treatments. *Appl. Surf. Sci.* **2008**, *254*, 1578–1582. [CrossRef]
26. Han, W.S.; Kim, Y.Y.; Kong, B.H.; Cho, H.K. Ultraviolet light emitting diode with *n*-ZnO:Ga/*i*-ZnO/*p*-GaN:Mg heterojunction. *Thin Solid Films* **2009**, *517*, 5106–5109. [CrossRef]
27. Kim, H.; Jin, C.; Park, S.; Lee, W.I.; Lee, C. Structure and luminescence properties of thermally nitrated Ga<sub>2</sub>O<sub>3</sub> nanowires. *Mater. Res. Bull.* **2013**, *48*, 613–617. [CrossRef]
28. Reshchikov, M.A.; Demchenko, D.O.; McNamara, J.D.; Fernández-Garrido, S.; Calarco, R. Green luminescence in Mg-doped GaN. *Phys. Rev. B* **2014**, *90*. [CrossRef]
29. Hofmann, D.M.; Meyer, B.K.; Alves, H.; Leiter, F.; Burkhard, W.; Romanov, N.; Kim, Y.; Krüger, J.; Weber, E.R. The red (1.8eV) luminescence in epitaxially grown GaN. *Phys. Status Solidi A Appl. Mater. Sci.* **2000**, *180*, 261–265. [CrossRef]
30. Glaser, E.R.; Carlos, W.E.; Braga, G.C.B.; Freitas, J.A., Jr.; Moore, W.J.; Shanabrook, B.V.; Henry, R.L.; Wickenden, A.E.; Koleske, D.D.; Obloh, H.; *et al.* Magnetic resonance studies of Mg-doped GaN epitaxial layers grown by organometallic chemical vapor deposition. *Phys. Rev. B* **2002**, *65*. [CrossRef]
31. Reshchikov, M.A.; Morkoç, H. Luminescence properties of defects in GaN. *J. Appl. Phys.* **2005**, *97*. [CrossRef]
32. You, W.; Zhang, X.D.; Zhang, L.M.; Yang, Z.; Bian, H.; Ge, Q.; Guo, W.X.; Wang, W.X.; Liu, Z.M. Effect of different ions implantation on yellow luminescence from GaN. *Physica B* **2008**, *403*, 2666–2670. [CrossRef]
33. Bouguerra, M.; Belkhir, M.A.; Chateigner, D.; Samah, M.; Gerbous, L.; Nouet, G. Blue and yellow luminescence of GaN nanocrystals-doped SiO<sub>2</sub> matrix. *Physica E* **2008**, *41*, 292–298. [CrossRef]
34. Sedhain, A.; Li, J.; Lin, J.Y.; Jiang, H.X. Nature of deep center emission in GaN. *Appl. Phys. Lett.* **2010**, *96*, 151902. [CrossRef]
35. Lai, B.T.; Lee, C.T.; Hong, J.D.; Yao, S.L.; Liu, D.S. Zinc oxide-based Schottky Diode prepared using radio frequency magnetron cosputtering system. *Jpn. J. Appl. Phys.* **2010**, *49*. [CrossRef]
36. Fang, Z.B.; Yan, Z.J.; Tan, Y.S.; Liu, X.Q.; Wang, Y.Y. Influence of post-annealing treatment on the structure properties of ZnO films. *Appl. Surf. Sci.* **2005**, *241*, 303–308. [CrossRef]
37. Liu, D.S.; Wu, C.Y.; Sheu, C.H.; Tsai, F.C.; Li, C.H. The preparation of piezoelectric ZnO films by RF magnetron sputtering for layered surface acoustic wave device application. *Jpn. J. Appl. Phys.* **2006**, *45*, 3531–3536. [CrossRef]



© 2015 by the authors; licensee MDPI, Basel, Switzerland. This article is an open access article distributed under the terms and conditions of the Creative Commons by Attribution (CC-BY) license (<http://creativecommons.org/licenses/by/4.0/>).